Radiation Physics and Chemistry 212 (2023) 111117

Contents lists available at ScienceDirect

Radiation Physics and Chemistry

journal homepage: www.elsevier.com/locate/radphyschem

Radiometric and stimulated luminescent characterization of Amazonian sediments from the Middle Rio Negro, Western Amazon

Sonia H. Tatumi [a,e,*], Márcio Yee [a], Emílio A.A. Soares [b], Jefferson J. de Souza [b], Emanuele D.O. Grudzin [a], Casimiro S. Munita [c], Rogério B. Ribeiro [c], Alvaro de Farias Soares [e], Noemi Aguiar Silva [a], Caroline P. Fernandes [a], Matheus T. Mathias [a], René R. Rocca [a], K.R. Nagabhushana [a], H.S. Lokesha [a], Marcelo S. Rocha [d], Luis A.C. Lopez [b], Diego W.P. Venâncio [b], Solange dos S. Costa [b]

[a] Universidade Federal de São Paulo, Instituto do Mar, Rua Carvalho de Mendonça, 144, 11070-100, Santos, SP, Brazil
[b] Universidade Federal do Amazonas, Departamento de Geociências, Av. Rodrigo Otavio 6200, 69077-000, Manaus, AM, Brazil
[c] Instituto de Pesquisas Energéticas e Nucleares, IPEN-CNEN/SP, Av. Prof. Lineu Prestes, 2242, 05508-000, São Paulo, SP, Brazil
[d] Universidade do Estado do Amazonas, Av.Djalma Batista, 3578, Flores, cep.69050-010, Manaus, Amazonas, Brazil
[e] University of São Paulo, Department of Electrical Engineering, Av. Prof. Luciano Gualberto, 158, 05508-080, São Paulo, SP, Brazil

ARTICLE INFO

Handling Editor: Piotr Ulanski

Keywords:
Fluvial sediment
Amazon basin
Radioactive isotopes
Neutron activation analysis
Optically stimulated luminescence
Phototransfer TL

ABSTRACT

The sediments were collected from paleodunes, river terraces, islands, and sand bars at Mariuá Archipelago, Rio Negro, Brazil. XRD analysis revealed that quartz is the predominant mineral along with a trace quantity of kaolinite. Neutron activation analysis of the sediments revealed the assembly of rare-earth elements, metals and semi-metals. The values of U and Th were found to be 3–5 ppm in paleodunes and 9–16 ppm in terraces, and K-40 concentration is below detectable limit. The OSL of quartz (dune) is composed of three components with decay times of 0.2, 11.0 and 350 s, respectively. This OSL emission is related to the TL peaks below 380 °C. Also, phototransferred TL is observed in the temperature range of 190–250 °C for a blue stimulation of 500 s. TL peaks kinetic parameters were calculated and discussed. The lifetimes of TL peaks at 272 and 355 °C are approximately 4.0×10^4 and 1.5×10^9 years, respectively. Using the conventional SAR protocol, 11 samples were dated, including two old paleodunes with ages of 124.4 and 169.7 ka, increasing the age interval of the site, the other samples were younger sediments, with ages between 0.39 and 53.9 ka.

1. Introduction

Optically Stimulated Luminescence (OSL) dating has been used to improve paleoenvironmental studies in different sedimentary environments due to the greater age limit and being used as a powerful tool in geological studies and characterization of associated events.

OSL dating helps to understand the sedimentation pattern and paleoclimatic changes that influenced the fluvial dynamics of the Solimões-Amazonas system, between the Purus and Madeira tributaries, in the upper Pleistocene - Holocene (Soares, 2007; Soares et al., 2010; Gonçalves Júnior et al., 2016; Passos et al., 2020; Fiore et al., 2014; Tatumi et al., 2020). Previous measurements of thermoluminescence (TL) dating of the sediments of paleodune field of the Rio Negro (a tributary of the Amazon River) (00°35′N, 63°14′W), and the analysis of ages spanning between 8 and 32 ka helped to understand the ecological changes during the last glacial maximum (Filho et al., 2002).

The Mariuá archipelago is considered the largest on the planet and is located at Rio Negro, Western Amazon. It has more than 1400 islands spread over 275 km in length and approximately 20 km in width, whose deposits can keep records of the main sedimentary, climatic and tectonic processes that influenced the stages of evolution of the Rio Negro basin for thousands of years. Few works on the mineralogical characterization of Amazon sediments were found in the literature. In addition to quartz, minerals such as goethite and kaolinite are reported (Allard et al., 2018; Albuquerque et al., 2017). Mineli and coworkers reported that, the TL of quartz from the Amazon has changed in the sensitivity of TL and OSL response (Mineli et al., 2021). Also, TL properties of quartz, taken from archaeological ceramics from the Amazon are reported (Cano et al.,

* Corresponding author. Universidade Federal de São Paulo, Instituto do Mar, Rua Carvalho de Mendonça, 144, 11070-100, Santos, SP, Brazil.
E-mail address: sonia.tatumi@unifesp.br (S.H. Tatumi).

https://doi.org/10.1016/j.radphyschem.2023.111117
Received 15 March 2023; Received in revised form 28 April 2023; Accepted 11 June 2023
Available online 19 June 2023
0969-806X/Published by Elsevier Ltd.

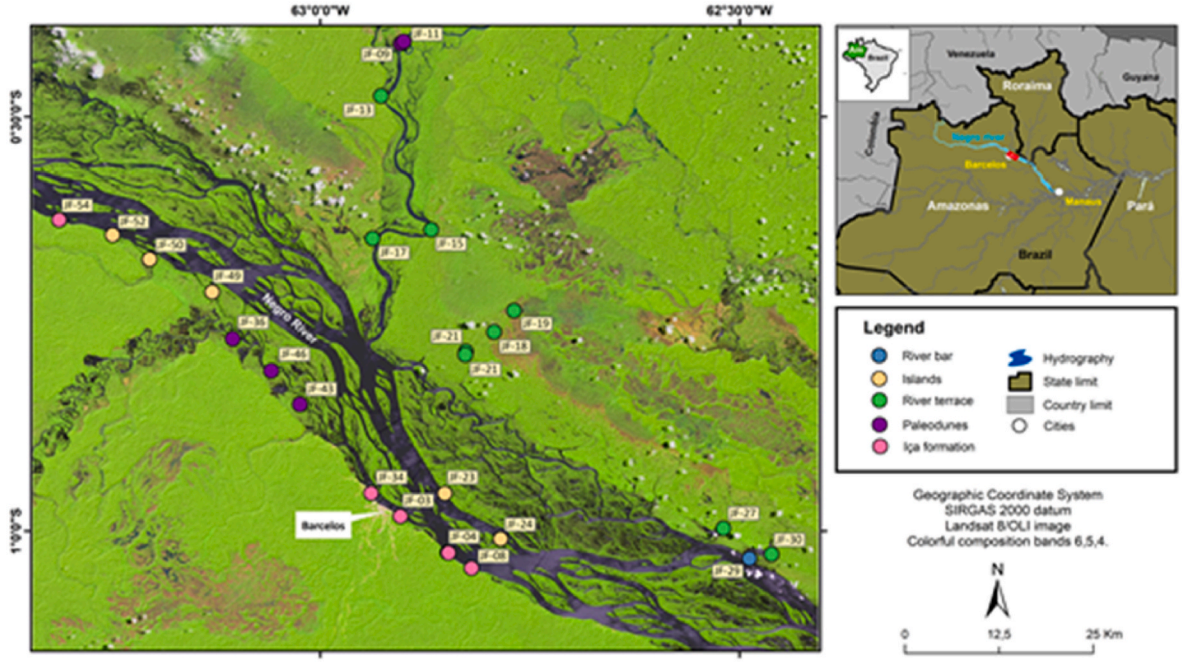

Fig. 1. Location map of the western portion of the Mariuá Archipelago, Middle Rio Negro, indicating the sites studied in the various geological units (Legend: Içá Formation, Paleodunes, Fluvial Terrace, Islands and River Bar).

2014). However, a detailed study on OSL and TL of quartz in the study region has not been found in the literature.

Point defects in quartz from sediments are mainly grouped into three types such as Aluminum-associated, hydrogen-related, and oxygen vacancies probed through various techniques including TL, OSL and EPR, etc., (Guzzo et al., 2006). Oxygen vacancies are called $E^{'}$- centers and the most important defects found in quartz are related to physical, optical and magnetic properties. The $E_1^{'}$- center is an oxygen vacancy with an unpaired electron located in one of the two non-equivalent Si atoms. The $E_2^{'}$ - center consists of an oxygen vacancy with an associated proton. $E_4^{'}$ - center is also an oxygen vacancy with a hybrid Si(I) atom. The optical absorption of $E^{'}$ - center bands appears in alpha-quartz only after irradiation. Various impurities such as alkali ion (M) Na^{+}, Li^{+} and K^{+} etc can enter the quartz network acting as modifiers and inducing non-bridging oxygen. These alkaline ions can diffuse along the c-axis channels (McKeever, 1985). The Al-alkali center is constituted by replacing the Si^{4+} ions with Al^{3+} ions. Optical absorption bands from this center can be observed at 620 (A_1 band), 480 (A_2 band) and 355 nm (A_3 band). Other centers such as Ge^{4+} and Ti^{4+} which may provide a site for the monovalent ion or electron too can also be found in quartz.

The blue emission luminescence in quartz and fused silica was observed when excited with 2 MeV electrons at 4.2 K which is associated with the relaxation of an exciton (Sigel, 1973). The samples also emitted blue light when excited with UV light at 4.2 K and 77 K. Radioluminescence bands at 440, 425 and 380 nm were observed in quartz and these emissions were thermally quenched below RT (Alonso et al., 1983). The 380 nm emission was associated with the recombination of electrons and unstable holes trapped at the Al center. Malik et al. (1981) observed TL peaks at 513 and 693 K with increasing irradiation temperature. Since the alkali ion can diffuse away from the Al-center during irradiation, resulting in the $(Al^{3+})^0$ center, which is the recombination center for electrons released from traps (Ge or Ti centers) and responsible for 450–470 nm emissions. However, as the crystal is natural the emission spectra vary due to its origin, which depends on the punctual defects and impurities concentrations. The studies continue using samples with different doping of alkali ions and concentrations as charge compensators in [AlO_4/M] center (Wintle and Adamiec, 2017).

This blue emission can be observed in TL data of quartz and several methods have been used in the evaluation of kinetic parameters of TL glow curves (Pagonis et al., 2006). Most of the methods are applicable for isolated peaks, but the glow curve deconvolution method has been used to acquire information about the kinetic parameters of each associated peak with the TL glow curve (Afouxenidis et al., 2012). To identify the number of peaks associated with the TL glow curve, the T_m-T_{stop}, thermal cleaning and fractional glow methods have been used. In the fractional glow method (Guckan et al., 2019), the sample was irradiated to the requisite dose only once and TL was recorded up to a specific temperature (example: 50 °C) and then cooled to room temperature. Further, TL was recorded to the next T_{stop} temperature (example: 60 °C). This procedure is repeated for different T_{stop} temperatures from 50 to 500 °C in the step of 10 °C. The activation energy of each fractional glow is calculated using the initial rise (IR) method (Guckan et al., 2019). In the IR method, the rising part of TL intensity not larger than 15% of the TL intensity at the peak maximum is used to calculate the activation of the glow (Pagonis et al., 2006). This method is applicable for TL from minerals extracted from sediments to understand the multiple trapping levels (broad TL glow curve). A plot of the activation energy of each fractional glow as a function of T_{stop} temperature gives a plateau representing a TL peak. Once the number of associated peaks is recognized from the fractional glow method, the complex glow curve deconvolution by using Kitti's general order kinetic equation (Afouxenidis et al., 2012).

In general, the geochronological studies of sediments the OSL dating was used. Though the OSL dating method is conceptualized and well established, depending on the predominant type of transport of the sediment, it needs to be altered and adapted. For example, in the case of river sediments, there can be a great fluctuation in the age calculation due to the different degrees of sunlight exposure to each grain. The grain that does not receive enough sunlight at the time of deposition may retain a certain residual amount of OSL signal, which will make its age higher than the true value. Therefore, in the present work, we apply the conventional OSL Single Aliquot Regenerative (SAR) protocol for quartz coarse grain to estimate the age of the sediments. The ages of collected set of sediments are obtained from a statistical model associated with the SAR protocol (Galbraith et al., 1999; Galbraith and Roberts, 2012; Peng

Table 1
Mineral composition of the sediments obtained from XRD analysis.

Sample	Depth (m)	Latitude/Longitude	Mineral	Score (%)	Observations
JF-01A	1.80	−0.9821831/−62.904349 1	Quartz	88	Içа Formation
			Hematite, syn	26	
			Kaolinite-montmorillonite	12	
JF-04F	1.80	−1.026449149/−62.8471382	Quartz low	93	Içа Formation
			Montmorillonite-15A	42	
			Baumite-1\ITT\RG [NR]	20	
JF-08C	2.10	−1.0449131/−62.8195346	Quartz-alpha	91	Içа Formation
			Kaolinite-montmorillonite	44	
JF-09A	1.20	−0.4113535546/−62.90358775	Quartz-alpha	80	Paleodune
			Quartz low	25	
JF-11A	3.00	−0.4091278815/−62.90047829	Quartz-alpha	86	Paleodune
JF-15A	1.90	−0.6362232249/−62.86774304	Quartz	79	River terrace
			Kaolinite-1\ITMd\RG	40	
			Cristobalite-beta (high)	11	
JF-17A	1.00	−0.6468551247/−62.93755614	Quartz, low	81	River terrace
			Kaolinite	68	
			Cryptohalite, syn	22	
JF-17B	3.00	−0.6468551247/−62.93755614	Quartz-alpha	87	River terrace
			Kaolinite 1Md	49	
JF-19A	0.20	−0.7340473808/−62.76886062	Quartz-alpha	92	River terrace
			Kaolinite-montmorillonite	59	
JF-19Ainf	3.00	−0.7340473808/−62.76886062	Quartz low	90	River terrace
			Kaolinite	57	
JF-19Asup	1.80	−0.7340473808/−62.76886062	Quartz-alpha	92	River terrace
			Baumite-1\ITT\RG [NR]	38	
			Kaolinite	43	
JF-29A	0.40	−1.033142491/−62.48803904	Quartz -alpha	84	River bar
			Marshite, syn	24	
			Microcline	28	
			Rustenburgite	41	
			Telluropalladinite	28	
JF-30B	1.00	−1.028035632/−62.46148988	Quartz-alpha	78	River terrace
			Kaolinite	35	
			Spinel (Li, Mg, Ti), syn	20	
MP-01	3.00	−1,0259335/-62,8480820	Quartz low, syn	68	River terrace- heavy mineral
			Ilmenite	42	
			Zircon	37	
			Rhodium, syn	20	

et al., 2013; Wintle and Murray, 2006). In this context, the focus of this work aims to study the deposits of the Mariuá Archipelago and the outcome relates to the aspects of source areas, the chronology of deposits and paleoclimatic events. Also, we studied the continuous wave CW-OSL and correlated it with the centers of thermoluminescence (TL) and their thermal stability.

2. Experimental

A total of 38 samples were collected from different depths in 25 locations from outcropping alluvial deposits in the western portion of the Mariuá Archipelago, Rio Negro. The location of the samples collected is marked on the map shown in Fig. 1. Here, among these 38 samples, 14 samples were characterized using XRD (Table 1). Another 17 samples were exclusively used for neutron activation analysis (Table 2). The Remaining 7 samples along with 4 samples (used for XRD analysis) were used for OSL dating (Table 4) and gamma spectroscopy analysis (Table 5).

X-Ray Diffraction (XRD) patterns of the collected sediments (natural) were performed using a Rigaku Miniflex 300 X-ray diffractometer with a source of CuK_{α} (1.5418 Å). The operating voltage and current are 30 kV and 10 mA, respectively.

The elemental composition of sediments was determined by Instrumental Neutron Activation Analysis (INAA). For INAA measurements, the sediments were ground in an agate mortar and pestle until to obtain the grains that pass through a 100–200 μm mesh sieve. The sieved samples were dried in an oven at 105°C for 24 h. Two series of measurements were carried out using Ge (hyperpure) detector (model: GX, 2020; make: Canberra) having a resolution of 1.90 keV at the 1332.49 keV gamma-peak of ^{60}Co, with S-100 MCA with 8192 channels. Na, K, La, and Yb were measured after 7 days of cooling time and Sc, Fe, Co, Cs, and Th after 25–30 days. Gamma spectra analysis was carried out using the Genie-2000 NAA processing procedure program from Canberra. NIST-SRM1633b Constituent Elements in Coal Fly Ash were used as standard.

Gamma spectroscopy measurements were carried out with an HPGe detector, Model Gx6020, calibrated through Japanese standard samples (JR-1, JG-1a, JB-3 and JG-3). Gamma spectroscopy measurements were carried with an HPGe detector, Model Gx6020, calibrated through japanese standard samples of ground (JR-1, JG-1a, JB-3 and JG-3). In this technique, the gamma-radiation spectra emitted by the samples were measured, which were compared to those of the standards. The peak intensities used for this analysis corresponding to the energies: 238 and 261 keV for Th; 295, 352, 1120 and 1764 keV for U; 1460 keV for the K-40. The samples were dried before measurements, the amount of water content in the sediment is determined, this data was used in the annual dose rate calculation corrections, then the mass of 100 g of sediment approximately were sealed in plastic pots and kept closed for two weeks before reading, in order to achieve electronic equilibrium and placed in the detector to be measured for 24 h each sample. Finally, the annual dose rates are evaluated with the U, Th and K-40 concentrations and the conversion table cited by Adamiec and Aitken (1998), the contributions of the cosmic radiations were calculated theoretically with of Prescott and Hutton (1994) equations.

For OSL dating the samples were collected in aluminium tubes of size 15 cm in length and 2.5 cm in diameter and the light exposed ends of the sediments from the tubes were discarded and unexposed sediments were chemically cleaned with H_2O_2 for 2 h to remove organic material. Then

Table 2
Major element and traces content of sediment obtained by Instrumental Neutron Activation Analysis.

Sample	Geographic.coordinate		Na %	K %	La	Sm	Yb	Lu	Sc	Cr	Fe %	Co	Rb	Cs	Ce	Eu	Hf	Ta	Th
JF 27A Terrace	−0.9977	−62.5201	0.017	0.42	31.60	4.94	2.35	0.51	8.07	34.94	1.22	3.20	27.47	2.20	40.71	0.48	37.42	1.34	14.56
JF 52B Island	−0.6436	−63.2488	0.082	1.06	32.49	3.58	3.16	0.50	7.43	40.74	0.87	2.19	61.24	3.60	50.21	0.68	23.79	1.77	11.00
JF 15B Terrace	−0.6373	−62.8688	0.040	0.64	23.05	3.48	1.82	0.30	7.01	49.80	1.15	1.50		1.58	38.26	0.26	10.14	1.07	8.89
JF 24A Island	−1.0106	−62.7858	0.12	1.69	42.62	5.67	3.06	0.57	7.98	24.09	0.80	3.13	80.04	3.85	62.05	0.62	24.53	1.07	13.53
JF 34A	−0.9554	−62.9404	0.09	1.28	42.16	6.17	3.73	0.61	12.08	46.04	1.02	7.38	60.14	6.44	81.41	1.47	15.03	1.07	11.13
JF 23A Island	−0.9556	−62.8526	0.13	2.19	25.98	2.72	2.67	0.52	4.90	20.99	0.39	1.26	73.47	2.39	37.30	0.33	30.56	1.28	9.73
JF 30A Terrace	−1.0290	−62.4626	0.021	0.57	26.55	1.50	2.59	0.53	6.52	33.30	0.58	2.09	49.02	1.70	45.48	0.46	37.19	1.49	13.54
JF 20A Terrace	−0.7841	−62.8273	0.011	0.40	66.96	4.31	1.53	0.30	11.45	69.41	1.67	5.39		4.02	72.88	0.62	12.57	3.19	23.31
JF 17B Terrace	−0.6479	−62.9386	0.014		53.10	6.18	1.93	0.38	12.75	62.48	1.51	4.45		3.54	74.09	0.57	16.08	3.39	22.69
JF 50A	−0.6728	−63.2048	0.080	0.98	26.29		2.86	0.49	5.80	28.28	0.70	1.75	28.36	2.93	47.85	0.42	21.84	0.89	9.66
JF 03B Island	−1.0270	−62.8492		1.06	64.11	6.49	4.37	0.67	14.69	56.79	1.20	2.58	54.07	6.19	112.12	1.78	11.89	1.28	15.11
JF 18A Terrace	−0.7608	−62.7937	0.013	0.33	28.97	2.94	2.97	0.54	8.61	42.44	8.15	3.31		3.40	35.84	0.36	38.33	1.18	17.30
JF 49B	−0.7124	−63.1300	0.067	0.75	34.34	6.88	3.69	0.68	8.13	42.04	0.88	2.38		4.82	49.22	0.63	20.96	1.02	10.47
JF 21A Terrace	−0.7882	−62.8281	0.014	0.50	35.74	2.57	2.36	0.48	8.84	50.04	13.17	4.18		4.02	36.89	0.46	35.12	1.59	16.99
JF 13B Terrace	−0.4759	−62.9286	0.030	0.32	37.03	0.91	2.92	0.55	8.17	36.74	0.58	1.73		1.97	59.00	0.77	31.51	1.17	11.43
JF 54B Içá	−0.6270	−63.3125	0.17	1.89	47.71	5.11	3.89	0.62	12.27	62.56	15.66	15.41	70.77	4.07	80.65	1.16	14.62	1.56	14.58
JF 19B Terrace	−0.7351	−62.7699	0.050	0.54	23.09		2.78	0.49	11.09	77.87	3.77	2.05	35.37	5.48	38.21	0.37	13.52	1.65	12.56

Table 3
Kinetic parameters obtained by TL deconvolution analysis of JF-09A for a dose of 100 Gy.

JF09A FOM = 1.76%	Peak1	Peak2	Peak3	Peak4	Peak5	Peak6
I_{max}	17000	9000	10000	23000	64000	34000
T_{max} (K)	150	194	272	355	386	473
E (eV)	0.91	1.00	1.30	1.63	1.64	2.05
s (s^{-1})	8.22×10^{8}	6.38×10^{8}	1.09×10^{10}	1.09×10^{11}	5.52×10^{10}	5.69×10^{11}
b	1.2	1.7	2.0	2.0	1.7	2.0
τ (a)	0.11	5.18	3.86×10^{4}	1.59×10^{9}	4.66×10^{9}	4.29×10^{15}

Table 4
Parameters obtained in dating the sediments. CAM = Central Age Model, *Minimum Age Model.

Sample	Water (%)	O.D. (%)/N	D_e (Gy) CAM	CAM Age (ka)	Obs.
JF9A	4	22/37	43.13 ± 2.41	124.4 ± 0.9	Paleodune
JF11A	2	19/38	42.72 ± 1.49	169.7 ± 1.0	Paleodune
JF17A	11	29/56	46.61 ± 2.00	22.7 ± 1.0	River terrace
JF27B	11	28/27	67.73 ± 3.88	31.2 ± 1.9	River terrace
JF29A	11	39/39	0.51 ± 0.04 *	0.39 ± 0.03*	Bar river
JF30B	9	29/30	114.22 ± 6.42	53.9 ± 3.2	River terrace
JF36A	4	27/34	9.06 ± 0.43	16.0 ± 1.0	Paleodune
JF36B	4	25/34	8.02 ± 0.31	15.3 ± 0.8	Paleodune
JF43C	2	18/40	4.29 ± 0.15	12.4 ± 0.8	Paleodune
JF46C	4	27/31	4.30 ± 0.22	12.3 ± 0.9	Paleodune
JF46E	6	23/32	5.41 ± 0.24	11.7 ± 0.7	Paleodune

Table 5
Content of natural radioisotopes found in sediments by gamma-spectroscopy (BDL – Beyond detection limit).

Sample	Depth (cm)	Th (ppm)	U (ppm)	K-40 (%)	AD (μGy/a)
JF9A	120	0.98 ± 0.04	0.53 ± 0.03	B.D.L.	347 ± 16
JF11A	264	0.75 ± 0.03	0.35 ± 0.02	B.D.L.	252 ± 12
JF17A	100	14.48 ± 0.49	3.93 ± 0.17	0.14 ± 0.01	2055 ± 39
JF27B	50	12.05 ± 0.41	4.19 ± 0.18	0.36 ± 0.01	2173 ± 39
JF29A	40	3.11 ± 0.12	1.44 ± 0.07	0.71 ± 0.02	1324 ± 27
JF30B	100	10.97 ± 0.40	4.03 ± 0.17	0.39 ± 0.01	2121 ± 39
JF36A	60	2.47 ± 0.10	0.94 ± 0.05	0.01 ± 0.01	567 ± 20
JF36B	90	1.87 ± 0.08	0.54 ± 0.03	0.11 ± 0.01	524 ± 18
JF43C	95	1.09 ± 0.05	0.44 ± 0.03	B.D.L.	347 ± 17
JF46C	80	1.04 ± 0.05	0.46 ± 0.03	B.D.L	351 ± 18
JF46E	50	1.22 ± 0.05	0.44 ± 0.03	0.11 ± 0.01	461 ± 19

the mixture is washed with distilled water and immersed in 30% HF for 2 h to remove carbonates and the outermost layer affected by alpha radiation. Then, the samples were immersed in 10% HCl for 2 h to remove fluorides formed in the HF bath and then thoroughly washed with distilled water. Then the samples are dried in a hot air oven maintained at 70 °C and the samples were sieved in order to collect grains (0.125 mm < x < 0. 150 mm). Therefore, it is confirmed that the OSL dating is performed only on quartz not polymineral sample.

OSL and TL measurements were carried out in an automated TL/OSL reader (Model Risø TL/OSL-DA-20), with blue light excitation (470 nm) and detected in the UV region using a Hoya U-340 optical filter. The samples were irradiated for the requisite dose with a $^{90}Y/^{90}Sr$ beta source having a dose rate of 0.067 Gy/s. TL glow curves were recorded at a heating rate of 5 K s^{-1}. The equivalent doses (D_e) were determined by using the SAR protocol (SAR, Wintle and Murray, 2006), using 48 aliquots (~3 mg of 125–150 μm) of the sample. The D_e results were passed with recycling (±10%) and recuperations (<5%) tests which were used to obtain the final D_e value for each sample. The final D_e value was calculated with the Age Model (Galbraith and Roberts, 2012), and the "NumOSL Program" (Peng et al., 2013). The Central Age Model (CAM) was adopted when the Overdispersion (OD) was below 30% and the Minimum Age Model (MAM) for OD was larger than 30%. A total of 11 samples are used for the estimation of age (Table 4).

3. Results and discussion

3.1. X-ray diffraction

XRD patterns of JF-04A, JF-09A, JF-17A, JF-19Asup, JF-29A and MP-01 samples are shown in Fig. 2. The mineral composition of the sediments was analysed using X'Pert HighScore Plus software with PDF2/2003 database from the International Centre for Diffraction Data (ICDD) and tabulated in Table 1. The paleodunes exhibit a predominance of quartz, the score ranging from 80 to 86%, the quartz concentration is varied from 88 to 93% for the Içá formation, 78–92% for the river terraces, and 84% for the sand bar samples. Another most common mineral is kaolinite found in a score range from 12 to 44% and 35–68% for Içá formation and river terraces, respectively. However, kaolinite was not found in the paleodunes and in the sand bar. Other minerals such as smectite and illite + chlorite were not found in the sediments. Guyot et al. (2007) detected smectite and illite + chlorite minerals in the collected samples nearby the region of Cuiumi River (−0.7523; −63.1117) and in the Demini River (−0.7358; −62.9243). The score value of kaolinite is 67 and 98%, respectively. They concluded that the sediments may consist weathered of rocks and soils. They also observed the presence of hematite, cristobalite, cryptohalite, microcline etc, in a lower percentage.

3.2. Instrumental neutron activation analysis

The results of INAA were transformed to log base10 to compensate for the large differences in magnitudes between the measured elements for the trace level and the larger ones. The log base 10 transformation of data before a multivariate statistical method is common. One reason for this is a belief that, within the raw materials of manufacture, elements have a natural log-normal distribution for which normality of the data is desirable. Another reason is that a logarithmic transformation tends to stabilize the variance of the variables and would thus give them approximately equal weight in an unstandardized multivariate statistical analysis. Table 2 shows the trace elements detected in the samples. The concentrations of La, Cr, Ce, Rb, and Hf were the highest in all the samples, followed by As, Sc, Th, and the elements Yb, Lu, Fe, Co, Cs, and Eu were in lower concentrations. Rare-earth elements have luminescence centers that may possibly be contributing to TL and OSL emissions

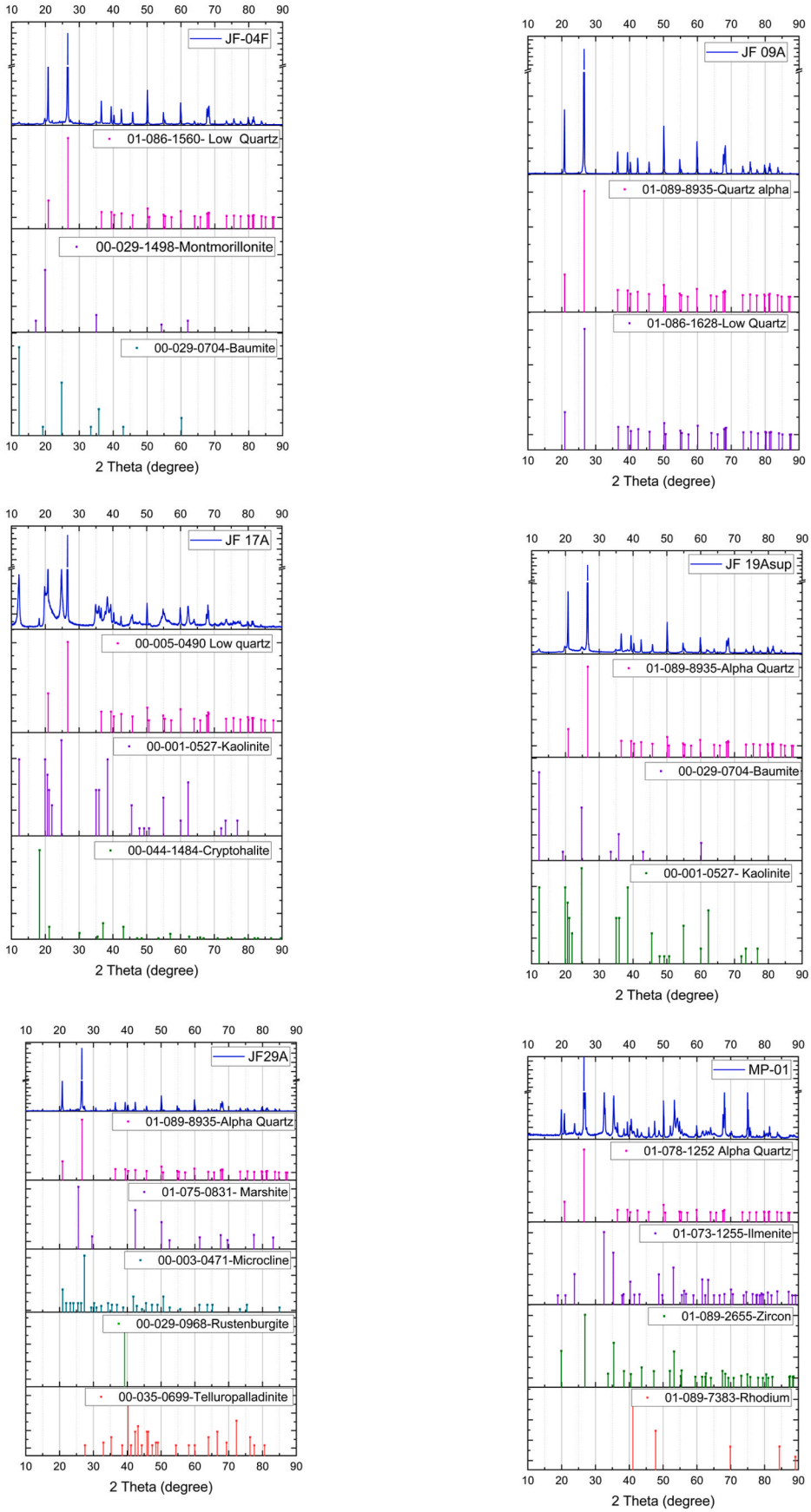

Fig. 2. Powder XRD patterns of JF-04F, JF09A, JF17A, JF19Asup, JF29A and MP01 samples.

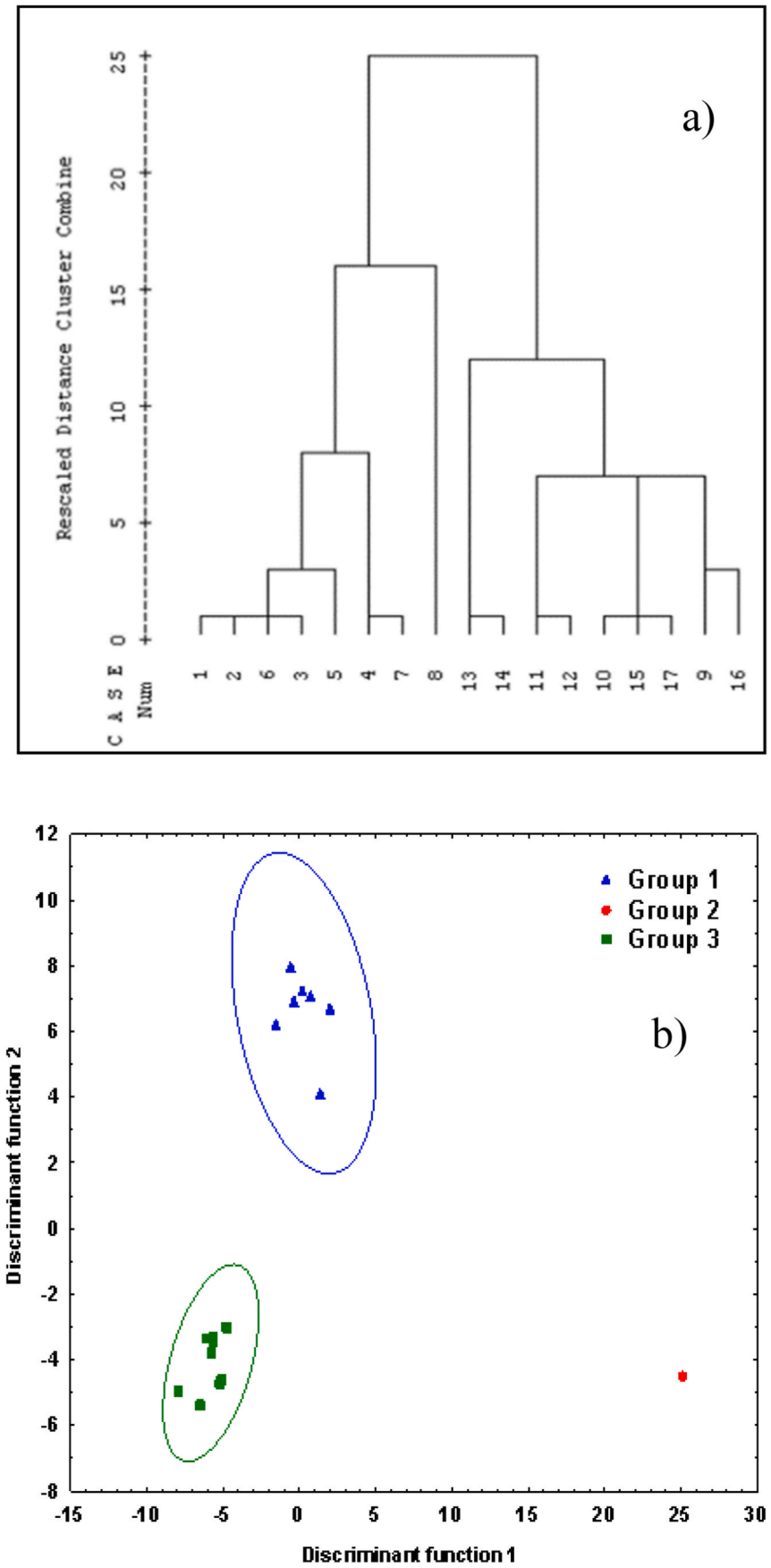

Fig. 3. (a) Dendrogram of 17 samples using Ward's method and squared Euclidean distance and (b) canonical discriminant functions for samples. The ellipses represent 95% confidence levels for samples inclusion into clusters.

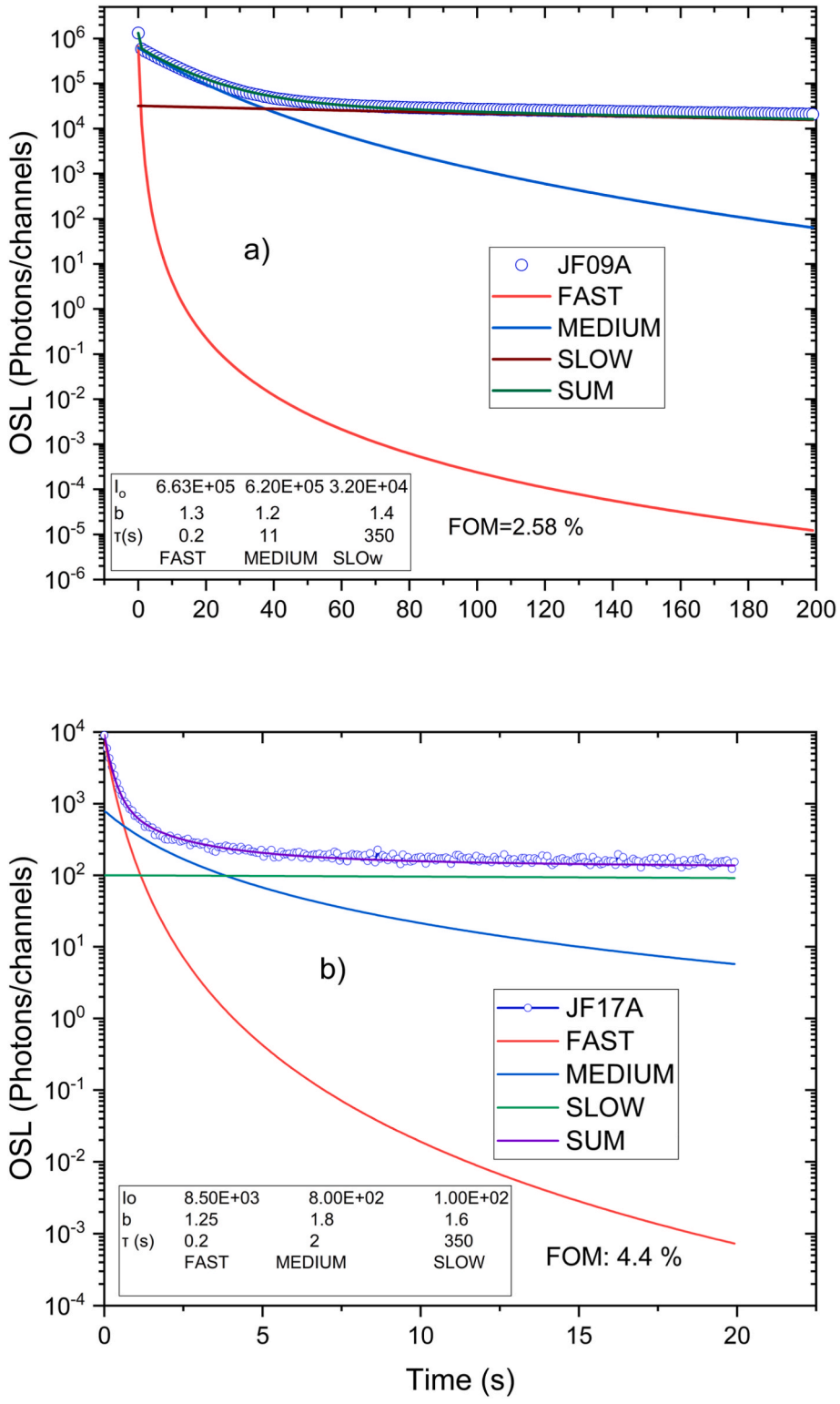

Fig. 4. Experimental and deconvoluted CW-OSL decay curves of quartz extracted from (a) paleodune (JF09A) and (b) river sediment (JF17A).

of the sediments.

Further, the results are subjected to cluster and discriminant analysis for studying the similarities and dissimilarities between the samples. Fig. 3(a) shows the dendrogram of INAA results of 17 samples, and the distance measured used was squared Euclidean distance. Visual inspection of the dendrogram is useful a method of identifying preliminary groups. The dendrogram suggests that the samples are classified into three groups (group 1: samples 1, 2, 6, 3, 5, 4 and 7; group 2: sample 8 and group 3: samples 13, 14, 11, 12, 10, 15, 17, 9 and 16). In order to confirm the compositional groups, the data were submitted for discriminant analysis. Fig. 3(b) shows the plot of discriminant function 1 versus discriminant function 2 wherein it is possible to see three groups.

3.3. *Optically stimulated luminescence*

Fig. 4 shows the typical CW-OSL response of the sediments from (a)

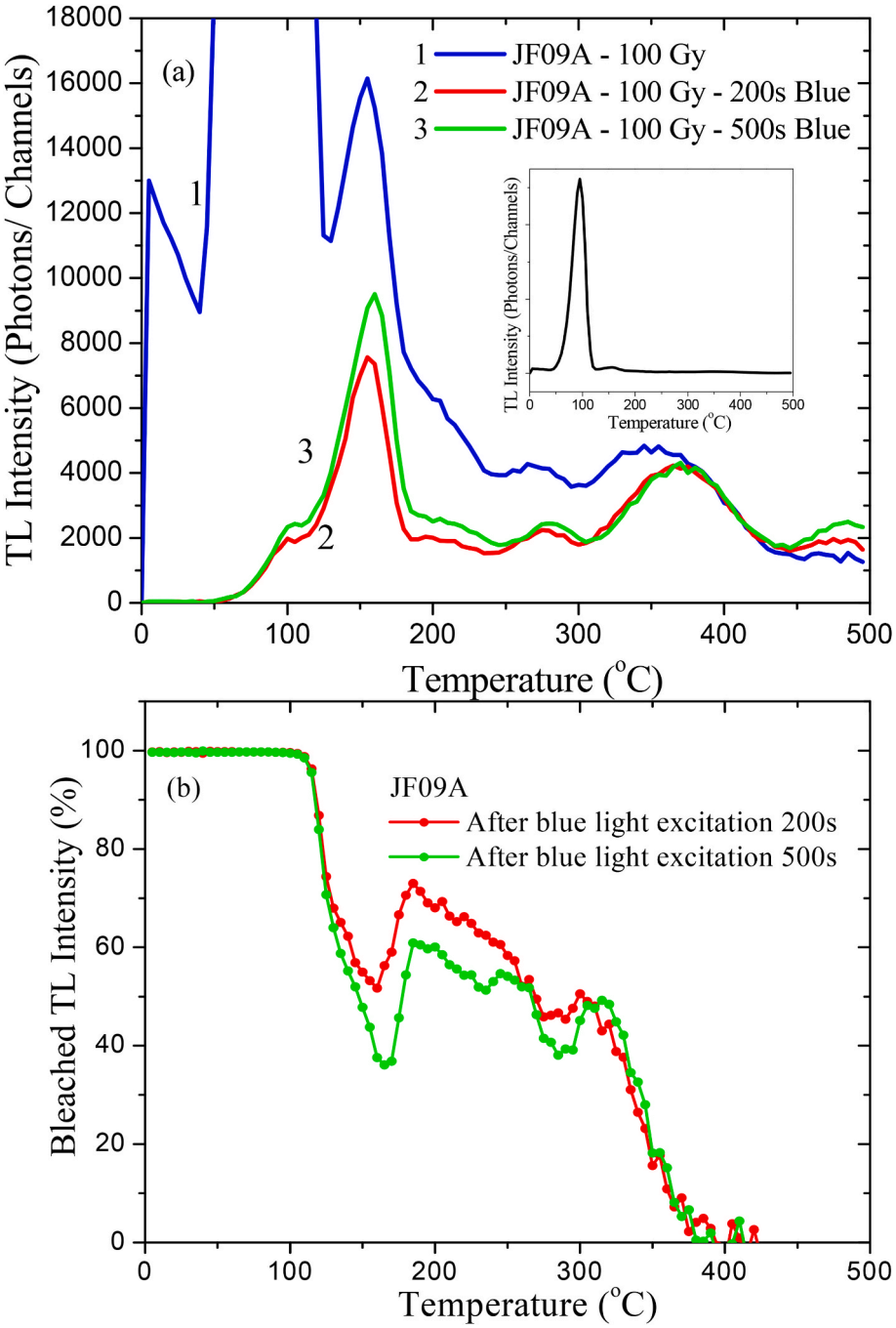

Fig. 5. (a) TL glow curves of quartz from JF09A sample irradiated with 100 Gy beta particles (blue), blue illumination for 200 s (red) and blue illumination for 500 s (green). (Inset: TL of the JF09A irradiated at 100 Gy), b) Variation of bleaching percentage of TL curves of blue light illumination.

paleodunes (JF-09A) and (b) river sediment (JF-17A). In order to determine the OSL decay components, the experimental OSL decay curves were deconvoluted using the general order kinetics equation (Afouxenidis et al., 2012). The equation is given below.

$$I(t) = I_0\left(1 + (b-1)\frac{t}{\tau}\right)^{\left(\frac{b}{b-1}\right)} \quad (1)$$

Where *I(t)* is the OSL intensity, I_0 is the initial intensity, b is the kinetic order and τ is the lifetime of the traps. The deconvoluted OSL curves of the JF-09A and JF-17A are shown in Fig. 4 (a) and (b) respectively. Both the OSL curves are fitted for fast, medium, and slow components and obtained kinetic parameters are given as an inset of the respective figures. The figure of merit of the deconvoluted curves is 2.5% and 4.4% for JF-09A and JF-17A samples, respectively which indicates a good fit between experimental and theoretical profiles. The lifetime decay of fast, medium and slow components is found to be (0.2, 11.0 and 350 s) and (0.2; 2.0 and 350 s) and corresponding order of kinetics (1.3, 1.2 and 1.4 s) and (1.25. 1.8 and 1.6) for JF-09A and JF-17A respectively.

3.4. Thermoluminescence

It is significant to figure out which part of the trap distribution corresponds to the OSL process in the material for dating and dosimetry. In order to correlate the TL centers with OSL, TL measurements were performed with beta irradiation. The TL curves are compared before and

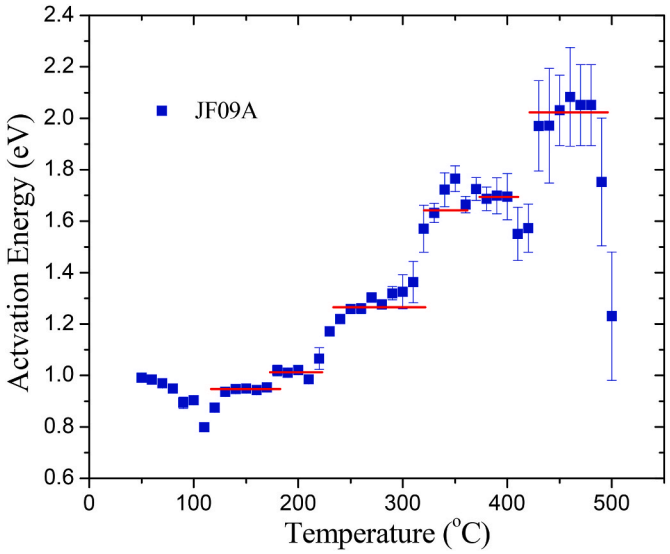

Fig. 6. Activation energies versus temperature (T_{stop}) of JF09A sample calculated using fractional glow curve data.

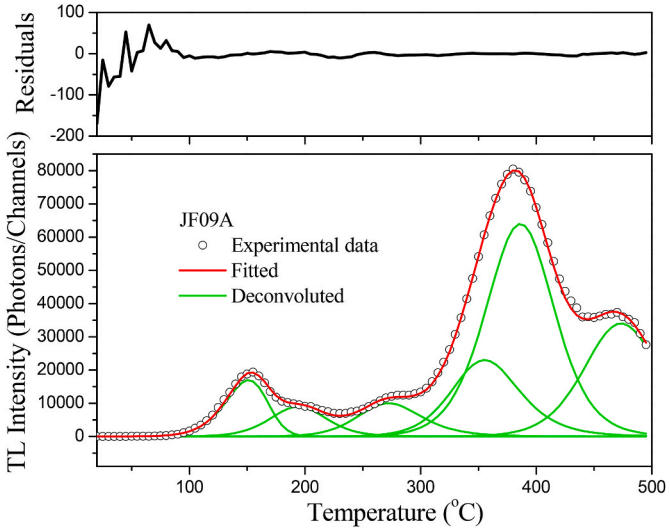

Fig. 7. Deconvoluted TL glow curves of JF09A sample. Inset: the residual TL as a function of temperature.

after the illumination with blue light (470 nm LEDs) to verify the change in intensities of the TL peaks. Fig. 5 (a) shows the TL glow curves of JF-09A. The blue color is curve recorded immediately after beta irradiation (100 Gy), the red and green color curves are measured on the irradiated samples illuminated with blue LED's (470 nm) for 200 s and 500 s, respectively. It is observed that the TL peak intensity decreases with 200 s illumination. Further, TL intensity increased for 500 s illumination due to the phototransfer of traps responsible for TL. The change in intensities of TL peaks is calculated for both the illumination times and given in Fig. 5 (b). It is observed that all peaks are affected by illumination, except the peak that appeared above 450 °C. The TL traps contribute to the OSL emission in different percentages from 50 to 100%. Kaya-Keles et al. (2019) studied TL, OSL and Electronic Paramagnetic Resonance (EPR) of alpha quartz crystal and concluded that several TL peaks can be correlated with the OSL components, which is in agreement with the present results. The effect of phototransfer in the temperature range 190–250 °C was observed in Fig. 5 (b) (green curves). The phototransfer is a well known process that occurs in many crystals such as fluorapatite (Soares et al., 2021), in synthetic materials Al_2O_3:Cr (Chithambo et al., 2023) and quartz which is used for geological dating (Folley and Chithambo, 2021; Bailiff et al., 1977).

The fractional glow curve (FGC) technique was used to determine the number of trap centers associated with the glow curve. The activation energies of each glow were calculated using the initial rise method (Pagonis et al., 2006). Fig. 6 shows the plot of activation energies versus T_{stop} for JF-09A sample. The FGC analysis confirms that, there are six plateaus around 0.94, 1.01, 1.26, 1.63, 1.69, and 2.03 eV which correspond to TL peaks at 150, 190, 270, 330, 390, and 460 °C respectively. The activation energy of the last TL peak has large uncertainties due to its low intensity.

TL glow curve of JF-09A was deconvoluted using a glow curve deconvolution method with general order kinetics equation (GOK) (Kitis et al., 1998) to estimate kinetic parameters such as activation energy (E), frequency factor (s) and order of kinetic (b) of the individual peak. Fig. 7 shows the deconvoluted TL curve of JF-09A**.** The figure of merit of the fit is below 2%, indicating a good fit. TL kinetic parameters obtained from the deconvoluted curve are tabulated in Table 3. The estimation of TL kinetic parameters for quartz extracted from sediments for dating is lacking in the literature. The kinetic parameters of the crystalline quartz were reported (Cuevas-Arizaca et al., 2020). Mineli et al. reported the variation of sensitivities of the OSL signal and 110 °C TL peak applied to provenance proxies (Mineli et al., 2021). The temperatures of TL peaks are generally close and independent of their origin. However, the E values are quite different, as they depend on the set of impurities and point defects found in the crystal lattice, in addition to the experimental reading parameters, such as heating rate, optical detection filters, etc.

The lifetime (τ) of TL traps can be calculated using the values of E and frequency factor (s) by the equation given below,

$$\tau = \frac{e^{\frac{E}{kT}}}{s} \tag{2}$$

The samples are stored at room temperature (23 °C). The calculated lifetime values for deconvoluted peaks are given in Table 3. As the lifetimes were calculated from equation (2), which is derived from 1st order Kinect model, the τ are approximate values. The τ value increased for peaks that appeared at higher temperatures. It was observed that the obtained OSL emission is a sum of charge contributions coming from

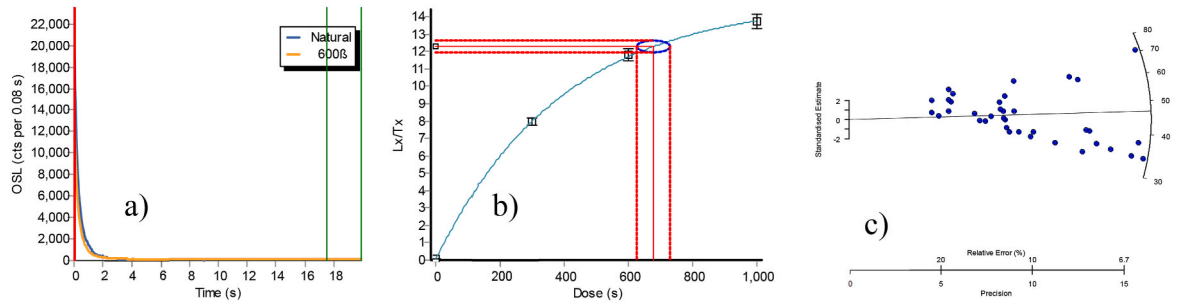

Fig. 8. (a) OSL signal, (b) OSL growth curve and (c) Radial Plot using minimum age model for JF09A sample.

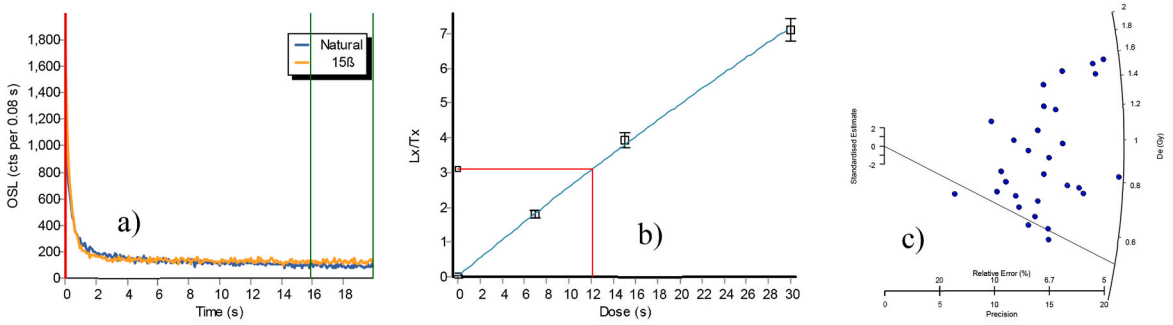

Fig. 9. (a) OSL signal, (b) OSL growth curve and (c) Radial Plot using minimum age model for JF29A sample.

several energy levels, so apply the preheating procedure to remove the contribution of shallow traps as proposed in the SAR protocol. In the present study, the OSL has a great contribution from the traps responsible for the quartz peaks at 355 and 386 °C and their τ values are around 10^9–10^{10} years. This fact is very important for dating the old sediments. The high temperature TL peak (473 °C) of JF-09A sample behaved anomalously, the lifetime of this peak is around 10^{15} years. Also, this peak remains the same after the illumination with blue light.

3.5. OSL dating

Fig. 8 shows OSL shine down curve, calibration curve using the SAR protocol and the "radial plot" graphs for determining equivalent doses (D_e) of JF-09A sample. The Radial plot was fitted with the Minimum Age Model for high over dispersion (*OD*) value as is shown in the Fig. 9. The JF-09A and JF-11A samples are the oldest dunes, with ages of 124.4 and 169.7 ka, respectively, these ages intervals are new in the study site and made the site older, and another set of ages of younger paleodunes (JF-36A, 36B, 43C, 46C and 46E) were found to be 11.7 to 16.0 ka. A previous study of the nearby dune field did not find old samples, the ages found covered the range of 8–32 ka (Filho et al., 2002; Tatumi et al., 2020). Samples from river terraces have an age span from 22.7 to 53.9 ka and the sediment barrier was the youngest with 0.39 ka and presented a large *OD* of 39%, all the values are given in Table 4. The radioactive content of the sediments obtained from gamma spectroscopy is tabulated in Table 5. The values of U and Th are low in the paleodunes 0.35–0.94 ppm of U and 0.75–2.47 ppm of Th; however, the river terraces have high values between 3.94 and 4.19 ppm of U and 10.97–14.48 ppm of Th. Generally, K-40 values are very low or almost zero, due to the low feldspar concentration in the region. With these values, annual dose rates were evaluated for the sites, in the case of paleodunes *AD* varied from 252 to 567 μGy/a and for river terrace from 2055 to 2173 μGy/a, this difference in *AD* values can be an evidence of the distinct origin of these sediments.

4. Conclusions

The sediments from different locations at Mariuá Archipelago were characterized and dated by OSL-SAR protocol successfully. XRD analysis confirmed that quartz is the predominant mineral followed by kaolinite in the Içá formation and terraces whereas the paleodunes and sand bar did not show the presence of kaolinite. The predominance of quartz, and kaolinite found in some samples were composed of eroded sediments by weathering. INAA showed a large assembly of rare-earth elements present in the sediments. The samples could be divided into three distinct groups using cluster and discriminant analysis. The OSL of quartz taken from the paleodunes and river sediment consists of three components. The OSL signals are related to TL peaks appearing below 380 °C, and blue light stimulation time above 500 s provides the phototransfer TL. The kinetic parameters of the traps and lifetimes are discussed. TL peaks (272 and 355 °C) are correlated to the OSL signal used for dating, whose lifetimes are about 4×10^4 and 1.5×10^9 years, respectively. The dunes have a lower concentration of radioisotopes. The oldest dues have AD rates from 252 to 347 μGy/a, the youngest dunes from 347 to 567 μGy/a and the terraces with much higher values of 2055–2173 μGy/a. The ages of two Aeolian dunes are 124.4 and 169.7 ka, the other samples had ages between 0.39 and 53.9 ka examined from conventional SAR protocol. Thus, increasing the age of the site is in question.

Declaration of competing interest

The authors declare that they have no known competing financial interests or personal relationships that could have appeared to influence the work reported in this paper.

Data availability

Data will be made available on request.

Acknowledgements

This work is jointly funded by *Fundação de Amparo à Pesquisa do Estado de São Paulo* (FAPESP - Process No: 2020/08592-8) and *Fundação de Amparo à Pesquisa do Estado do Amazonas* (FAPEAM). The authors (UNIFESP) also acknowledge CAPES-PrInt N°. 88881.311044/2018-00 and CNPq N°. 303665/2019-0. The authors express their sincere thanks to Mr. Mailson Trindade de Olivera, Escola Superior de Tecnologia, Universidade do Estado do Amazonas, Barcelos, AM, Brazil for his help during the sample collection.

References

Adamiec, G., Aitken, M.J., 1998. Dose-rate conversion factors: update. Ancient TL 16, 37–50.

Afouxenidis, D., Polymeris, G.S., Tsirliganis, N.C., Kitis, G., 2012. Computerised curve deconvolution of TL/OSL curves using a popular spreadsheet program. Radiat. Protect. Dosim. 149, 363–370. https://doi.org/10.1093/rpd/ncr315.

Albuquerque, M.F.S., Horbe, A.M.C., Botelho, N.F., 2017. Genesis of manganese deposits in southwestern Amazonia: mineralogy, geochemistry and paleoenvironment. Ore Geol. Rev. 89, 270–289. https://doi.org/10.1016/J.OREGEOREV.2017.06.012.

Allard, T., Gautheron, C., Riffel, S.B., Balan, E., Soares, B.F., Pinna-Jamme, R., Derycke, A., Morin, G., Bueno, G.T., Nascimento, N., 2018. Combined dating of goethites and kaolinites from ferruginous duricrusts. Deciphering the Late Neogene erosion history of Central Amazonia. Chem. Geol. 479, 136–150. https://doi.org/10.1016/j.chemgeo.2018.01.004.

Alonso, P.J., Halliburton, L.E., Kohnke, E.E., Bossoli, R.B., 1983. X-ray-induced luminescence in crystalline SiO_2. J. Appl. Phys. 54, 5369–5375. https://doi.org/10.1063/1.332715.

Bailiff, I.K., Bowman, S.G.E., Mobbs, S.F., Aitken, M.J., 1977. The phototransfer technique and its use in thermoluminescence dating. J. Electrost. 3, 269–280. https://doi.org/10.1016/0304-3886(77)90099-7.

Cano, N.F., Munita, C.S., Watanabe, S., Barbosa, R.F., Chubaci, J.F.D., Tatumi, S.H., Neves, E.G., 2014. OSL and EPR dating of pottery from the archaeological sites in Amazon Valley, Brazil. Quat. Int. 352, 176–180. https://doi.org/10.1016/j.quaint.2013.05.042.

Chithambo, M.L., Shinsho, K., Polymeris, G.S., 2023. Properties of phototransferred thermoluminescence of Al_2O_3:Cr. Phys. B Condens. Matter 650, 414576. https://doi.org/10.1016/j.physb.2022.414576.

Cuevas-Arizaca, E.E., Rondón, M.R., Rocca, R.R., Gomes, M.B., Cortez, B., Gonzales-Lorenzo, C.D., Takara, J.H., Rao, T.G., Cano, N.F., Chubaci, J.F.D., Campos, L.L., Watanabe, S., 2020. Study of thermoluminescence of green quartz pellets for low dose dosimetry. Radiat. Phys. Chem. 177, 109142 https://doi.org/10.1016/j.radphyschem.2020.109142.

Filho, A.C., Schwartz, D., Tatumi, S.H., Rosique, T., 2002. Amazonian paleodunes provide evidence for drier climate phases during the late pleistocene–holocene. Quat. Res. (Tokyo) 58 (2), 205–209. https://doi.org/10.1006/qres.2002.2345.

Fiore, M., Soares, E.A.A., Mittani, J.C.R., Yee, M., Tatumi, S.H., 2014. OSL dating of sediments from Negro and Solimões rivers – Amazon, Brazil, radiat. Phys. Chem. 95, 113–115. https://doi.org/10.1016/j.radphyschem.2012.12.041.

Folley, D.E., Chithambo, M.L., 2021. Analysis of thermoluminescence and phosphorescence related to phototransfer in natural quartz. J. Lumin. 238, 118217 https://doi.org/10.1016/j.jlumin.2021.118217.

Galbraith, R.F., Roberts, R.G., Laslett, G.M., Yoshida, H., Olley, J.M., 1999. Optical dating of single and multiple grains of quartz from Jinmium rock shelter, northern Australia: Part I, experimental design and statistical models. Archaeometry 41 (2), 339–364. https://doi.org/10.1111/j.1475-4754.1999.tb00987.x.

Galbraith, R.F., Roberts, R.G., 2012. Statistical aspects of equivalent dose and error calculation and display in OSL dating: an overview and some recommendations. Quat. Geochronol. 11, 1–27. https://doi.org/10.1016/j.quageo.2012.04.020.

Gonçalves Júnior, E.S., Soares, E.A.A., Tatumi, S.H., Yee, M., Mittani, J.C.R., 2016. Pleistocene-holocene sedimentation of solimões-amazon fluvial system between the tributaries Negro and Madeira, central Amazon. Braz. J. Genet. 46 (2), 167–180. https://doi.org/10.1590/2317-488920162016009.

Guckan, V., Ozdemir, A., Altunal, V., Yegingil, I., Yegingil, Z., 2019. Studies of blue light induced phototransferred thermoluminescence in $CaSO_4$:Mg. Nucl. Instrum. Methods Phys. Res. Sect. B Beam Interact. Mater. Atoms 448, 31–38. https://doi.org/10.1016/j.nimb.2019.03.058.

Guyot, J.L., Jouanneau, J.M., Soares, L., Boaventura, G.R., Maillet, N., Lagane, C., 2007. Clay mineral composition of river sediments in the Amazon Basin. Catena 71 (Issue 2), 340–356. https://doi.org/10.1016/j.catena.2007.02.002.

Guzzo, P.L., Khoury, H.J., Souza, C.P., Souza, A.M., Schwartz, M.O.E., Azevedo, W.M., 2006. Defect analysis in natural quartz from Brazilian sites for ionising radiation dosimetry. Radiat. Protect. Dosim. 119, 168–171. https://doi.org/10.1093/rpd/nci573.

Kaya-Keleş, Ş., Polymeris, G.S., Meriç, N., 2019. A component resolved study on the stable signal of Merck α-quartz: tentative correlation among TL peaks, OSL components and EPR signals. Nucl. Instrum. Methods Phys. Res. Sect. B Beam Interact. Mater. Atoms 458, 44–56. https://doi.org/10.1016/j.nimb.2019.07.029.

Kitis, G., Gomez-Ros, J.M., Tuyn, J.W.N., 1998. Thermoluminescence glow-curve deconvolution functions for first, second and general orders of kinetics. J. Phys. D Appl. Phys. 31, 2636–2641. https://doi.org/10.1088/0022-3727/31/19/037.

Malik, D.M., Kohnke, E.E., Sibley, W.A., 1981. Low-temperature thermally stimulated luminescence of high quality quartz. J. Appl. Phys. 52, 3600–3605. https://doi.org/10.1063/1.329092.

McKeever, S.W.S., 1985. Thermoluminescence of Solids. Cambridge University Press.

Mineli, T.D., Sawakuchi, A.O., Guralnik, B., Lambert, R., Jain, M., Pupim, F.N., del Rio, I., Guedes, C.C.F., Nogueira, L., 2021. Variation of luminescence sensitivity, characteristic dose and trap parameters of quartz from rocks and sediments. Radiat. Meas. 144, 106583 https://doi.org/10.1016/j.radmeas.2021.106583.

Pagonis, V., Kitis, G., Furetta, C., 2006. Numerical and Practical Exercises in Thermoluminescence, vol. 233. Springer Science+Business Media, Inc., Spring Street, New York, NY 10013, USA https://doi.org/10.1007/0-387-30090-2.

Passos, M.S., Soares, E.A., Tatumi, S.H., Yee, M., Mittani, J.C., Hayakawa, E.H., Salazar, C., 2020. Pleistocene-Holocene sedimentary deposits of the Solimões-Amazonas fluvial system, Western Amazonia. J. South Am. Earth Sci. 98, 102455 https://doi.org/10.1016/j.jsames.2019.102455.

Peng, J., Dong, Z.B., Han, F.Q., Long, H., Liu, X.J., 2013. R package numOSL: numeric routines for optically stimulated luminescence dating. Ancient TL 31 (2), 41–48.

Prescott, J.R., Hutton, J.T., 1994. Cosmic ray contributions to dose rates for luminescence and ESR dating: large depths and long-term time variations. Radiat. Meas. 23 (2–3), 497–500. https://doi.org/10.1016/1350-4487(94)90086-8.

Sigel, G.H., 1973. Ultraviolet spectra of silicate glasses: a review of some experimental evidence. J. Non-Cryst. Solids 13, 372–398. https://doi.org/10.1016/0022-3093(74)90002-7.

Soares, E.A.A., 2007. Depósitos pleistocenos da região de confluência dos rios Negro e Solimões, porção oeste de Bacia do Amazonas. Ph.D. Thesis. Universidade de São Paulo, São Paulo, Brazil. https://doi.org/10.11606/T.44.2007.tde-14082008-141522.

Soares, E.A.A., Tatumi, S.H., Riccomini, C., 2010. OSL age determinations of Pleistocene fluvial deposits in Central Amazonia. An. Acad. Bras. Cienc. 82 (3), 691–699. https://doi.org/10.1590/S0001-37652010000300017.

Soares, A. de F., Tatumi, S.H., Courrol, L.C., Barbosa, R.F., Ramachandraiah, N.K., 2021. Studies on luminescence properties and photo-thermo transfer phenomena in fluorapatite. Radiat. Phys. Chem. 201, 110490 https://doi.org/10.1016/j.radphyschem.2022.110490.

Tatumi, S.H., Rossetti, D. de F., Soares, E.A.A., 2020. Optically Stimulated Luminescence (OSL) Dating in the Amazonian Wetlands. Cambridge Scholars Publishing, 2020. ISBN (13): 978-1-5275-5430-6.

Wintle, A.G., Murray, A.S., 2006. A review of quartz optically stimulated luminescence characteristics and their relevance in single-aliquot regeneration dating protocols. Radiat. Meas. 41 (4), 369–391. https://doi.org/10.1016/j.radmeas.2005.11.001.